II. Experimental Procedure

(1) Sample Preparation

All the samples were synthesized by a solid-state reaction method with starting materials of $SrCO_3$(A.R.), In_2O_3(99.995%), Er_2O_3 (99.995%), Yb_2O_3(99.995%). The samples of $SrIn_2O_4$: $0.1Yb^{3+}/0.01Er^{3+}$ with sintering temperatures (1100°C, 1200°C, 1300°C, 1400°C, and 1500°C) were prepared to exploring the synthesis route, and $0.1Yb^{3+}/x Er^{3+}$ (x = 0.002, 0.005, 0.01, 0.03, 0.05) codoped, single Er^{3+} or Yb^{3+}-doped $SrIn_2O_4$ were synthesized at 1400°C to discuss the structure and luminescent properties of $SrIn_2O_4$-based UC phosphors. Some $CaIn_2O_4$-based samples were also prepared by using this method. Starting materials were weighted, mixed, and grounded in an agate mortar according to stoichiometric ratio. After all the materials were ground thoroughly, the mixtures were placed into alumina crucibles and then synthesized at the above-mentioned temperatures (1100°C, 1200°C, 1300°C, 1400°C, and 1500°C) for 3 h, with the heating rate of 5°C/min. These samples were cooled to room temperature naturally. After that, all the samples were washed for three times by the deionized water and dried for the following measurement.

(2) Characterization

X-ray diffraction measurement (D8 Advance diffractometer, Bruker Corporation, Karlsruhe, Germany, with CuK_α and linear VANTEC detector, λ = 0.15406 nm, 40 kV, 30 mA) was used to examine the phase composition and for the structure refinement. The powder diffraction data for Rietveld analysis were collected on the 2θ range 5°–100° with the step size of 0.02°, and the counting time was 3 s per step. Rietveld refinement was performed by using TOPAS 4.2 (Bruker Corporation).[26] The morphology of samples was characterized by a field-emission scanning electron microscopy (JSM-7001F; JEOL, Tokyo, Japan). The UC luminescent spectra were recorded on a Hitachi F-4600 spectrophotometer equipped with an external power-controllable 980 nm semiconductor laser (Beijing Viasho Technology Company, Beijing, China) as the excitation source. The Fourier-transform infrared spectroscopy spectra (FTIR) were recorded with PerkinElmer Spectrum 100 (Waltham, MA). Diffuse reflection spectra were measured on a UV-vis-NIR spectrophotometer (Shimadzu UV-3600, Kyoto, Japan) attached to an integral sphere, and $BaSO_4$ was used as a reference standard. All the measurements were carried out at room temperature.

III. Results and Discussion

To optimize the synthesis temperature of $SrIn_2O_4$ compounds doped with stoichiometric $0.1Yb^{3+}/0.01Er^{3+}$, the phase composition of as-prepared samples at different temperatures (1100°C–1500°C) were analyzed, and their XRD patterns are drawn in Fig. 1(a) and compared with the standard PDF diffraction lines of $SrIn_2O_4$ (JCPDS No.72-0801). The UC luminescent properties of these compounds were then measured, and the corresponding UC luminescence spectra under 980 nm laser excitation are shown in Fig. 1(b). The inset in Fig. 1(b) depicts the UC emission intensities (Er^{3+}, at 663 nm) upon different sintering temperatures. It is easy to find that the XRD patterns of samples from 1200°C to 1500°C fit well with the standard PDF diffraction lines of $SrIn_2O_4$. This result demonstrates that pure-phase structure of $SrIn_2O_4$ compounds were synthesized successfully. No other phases of Er and Yb ions can be detected, illustrating that the doped Er^{3+} and Yb^{3+} were well dissolved into the $SrIn_2O_4$ host lattice. From Fig. 1(b), obvious visible emissions at around 550 and 663 nm were observed, indicates Yb^{3+}/Er^{3+}-doped $SrIn_2O_4$ compounds with excellent UC luminescent properties have been prepared successfully.

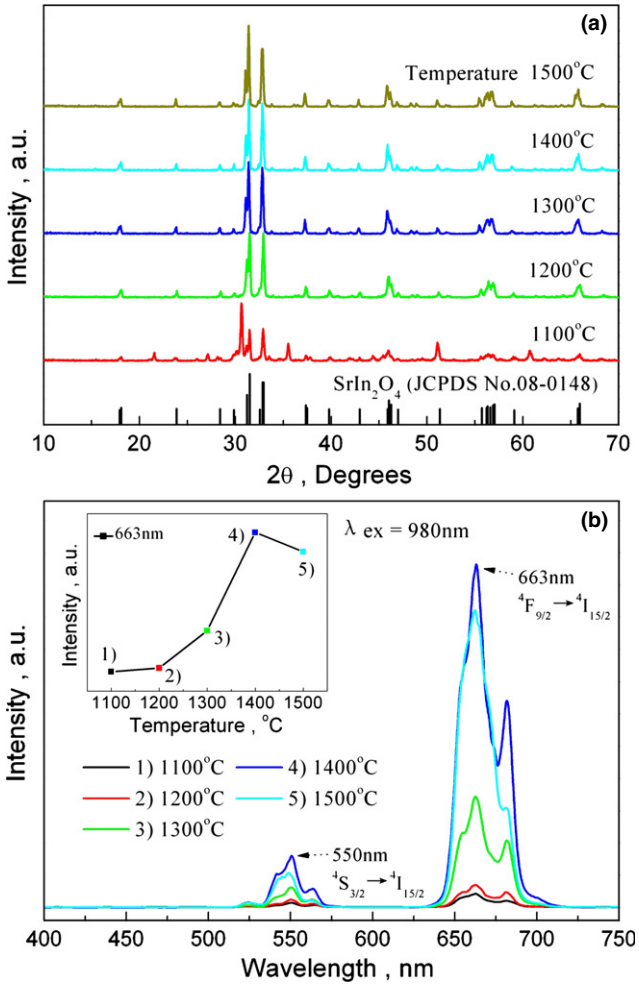

Fig. 1. (a) XRD patterns of $0.1Yb^{3+}/0.01Er^{3+}$-doped $SrIn_2O_4$ compounds with different sintering temperatures (1100°C, 1200°C, 1300°C, 1400°C, and 1500°C) and the standard PDF diffraction lines of $SrIn_2O_4$; (b) UC luminescence spectra of these corresponding samples under 980 nm laser excitation, and the inset shows the variation in UC emission intensities (Er^{3+}, at 663 nm) upon different sintering temperatures.

1400°C is the suitable temperature for gaining these kinds of phosphors.

Figures 2(a) and (b) show the SEM images of the $0.1Yb^{3+}/0.01Er^{3+}$-doped $SrIn_2O_4$ sample that sintered at 1400°C, and Fig. 2(b) is the enlarged part of (a). The grains are relatively regular and well-faceted with size of around 2–4 μm.

Yb^{3+}/Er^{3+} codoped ($SrIn_2O_4$: $0.1Yb^{3+}/xEr^{3+}$, x = 0.002, 0.005, 0.01, 0.03, 0.05) and single Er^{3+}-doped ($SrIn_2O_4$: $0.01Er^{3+}$) $SrIn_2O_4$ compounds were also prepared at the optimal temperature of 1400°C. Figures 3(a) and (b) show the Rietveld refinement plots of $SrIn_2O_4$:$0.1Yb^{3+}/0.01Er^{3+}$ (1) and $SrIn_2O_4$:$0.01Er^{3+}$ (2), respectively. All peaks of compound (1) were indexed by orthorhombic cell (*Pnma*) with parameters close to those earlier reported for $SrIn_2O_4$.[13] Almost all peaks of compound (2) were indexed by *Pnma* orthorhombic cell as well, and only several small peaks belongs to the impurity In_2O_3 phase [6.2(2) wt%]. Therefore, crystal structure of $SrIn_2O_4$ was taken as starting model for Rietveld refinement.

In the structure of $SrIn_2O_4$, there are one Sr site and two In sites. The dopant ions can be substituted in all of them. First of all, we tried to place Yb^{3+} and Er^{3+} ions in the Sr site. However, Rietveld refinement showed that the thermal parameters of Sr ion were not good in this case, and some discrepancies were found in difference plots. After that it was decided to test another model with Yb^{3+} and Er^{3+} ions in

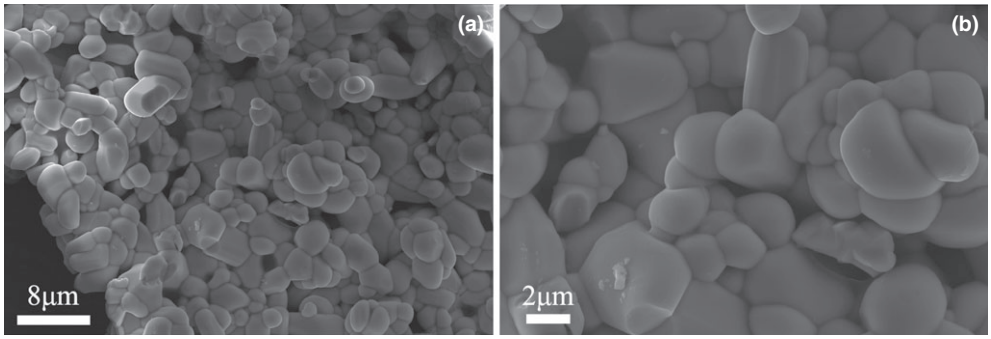

Fig. 2. (a) SEM images of the $0.1Yb^{3+}/0.01Er^{3+}$-doped $SrIn_2O_4$ sample; (b) enlarge part of (a).

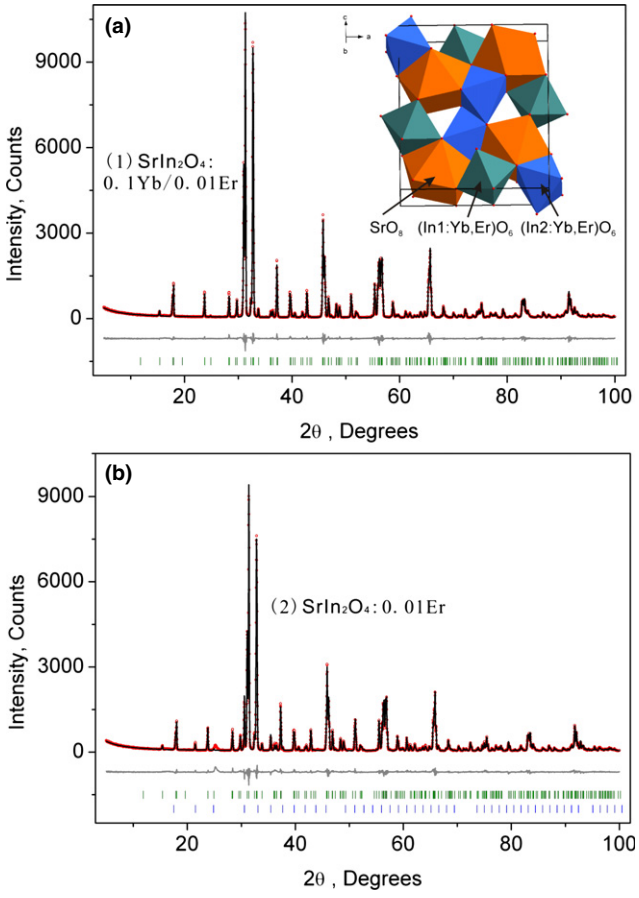

Fig. 3. (a) Difference Rietveld plot of $SrIn_2O_4$: $0.1Yb^{3+}/0.01Er^{3+}$ (1) and crystal structure of $SrIn_2O_4$:Yb^{3+}/Er^{3+}; (b) Difference Rietveld plot of $SrIn_2O_4$: $0.01Er^{3+}$ (2), impurity phase of In_2O_3 are marked by lowest row of blue sticks.

In1 and In2 sites. The R-factors became smaller in this second refinement (Table I, Fig. 3), all thermal parameters had good values (Table II) and bond distances were in good range (Table III). So it is reasonable to allocate Yb^{3+} and Er^{3+} in In1, 2 sites instead of Sr sites. Moreover, from ionic radii IR (Yb^{3+}, CN=6-8) = 0.868–0.985 Å, IR (Er^{3+}, CN = 6–8) = 0.89–1.004 Å, IR (In^{3+}, CN = 6) = 0.8 Å, IR (Sr^{2+}, CN = 8) = 1.26 Å,[14] one can conclude that if Yb^{3+}/Er^{3+} ions incorporate in Sr site then the unit cell volume should decrease, but if Yb^{3+}/Er^{3+} dopants incorporate in In sites then cell volume should increase. It was found that compound (1) with bigger dopant concentration has larger value of cell volume in comparison with compound (2) (Table I), so this is in good agreement with suggestion that Yb^{3+}/Er^{3+} ions are in In1/In2 sites instead of Sr site. In addition, it was found that compound (2) has bigger cell volume (V = 369.14 Å^3) in comparison with pure compound (V = 366.67 Å^3),[13] so Er^{3+} also incorporated in In1, 2 sites instead of Sr site. The final crystal structure of Yb^{3+}/Er^{3+}-doped $SrIn_2O_4$ is shown in Fig. 3(a).

Table I. Main Parameters of Processing and Refinement of the $SrIn_2O_4$: $0.1Yb^{3+}/0.01Er^{3+}$ (1) and $SrIn_2O_4$: $0.01Er^{3+}$ (2)

Compound	$SrIn_2O_4$: $0.1Yb^{3+}/0.01Er^{3+}$ (1)	$SrIn_2O_4$: $0.01Er^{3+}$ (2)
Sp.Gr.	*Pnma*	*Pnma*
a, Å	9.8527(1)	9.8317(1)
b, Å	3.27418(4)	3.26623(5)
c, Å	11.5221(1)	11.4950(2)
V, Å^3	371.698(7)	369.14(1)
Z	1	1
2θ-interval, °	5–100	5–100
Number of reflections	233	231
Number of parameters of refinement	57	65
R_{wp}, %	7.03	9.61
R_p, %	4.97	6.12
R_{exp}, %	6.65	6.76
χ^2	1.06	1.42
R_B, %	1.73	2.67

Table II. Fractional Atomic Coordinates and Isotropic Displacement Parameters (Å^2) of Compounds (1) and (2)

	x	*y*	*z*	B_{iso}	Occ.
$SrIn_2O_4$: $0.1Yb^{3+}/0.01Er^{3+}$ (1)					
Sr	0.24503 (16)	0.25	0.65203 (11)	0.63 (6)	1
In1	0.08051 (10)	0.25	0.39328 (8)	0.51 (6)	0.945
Yb1	0.08051 (10)	0.25	0.39328 (8)	0.51 (6)	0.05
Er1	0.08051 (10)	0.25	0.39328 (8)	0.51 (6)	0.005
In2	0.57073 (10)	0.25	0.61145 (7)	0.42 (6)	0.945
Yb2	0.57073 (10)	0.25	0.61145 (7)	0.42 (6)	0.05
Er2	0.57073 (10)	0.25	0.61145 (7)	0.42 (6)	0.005
O1	0.2859 (8)	0.25	0.3353 (8)	0.94 (12)	1
O2	0.1195 (8)	0.75	0.5223 (7)	0.94 (12)	1
O3	0.0176 (10)	0.75	0.2852 (7)	0.94 (12)	1
O4	0.4188 (9)	0.75	0.5804 (7)	0.94 (12)	1
$SrIn_2O_4$: $0.01Er^{3+}$ (2)					
Sr	0.2452 (2)	0.25	0.65337 (16)	0.38 (9)	1
In1	0.08099 (15)	0.25	0.39406 (11)	0.24 (9)	0.995
Er1	0.08099 (15)	0.25	0.39406 (11)	0.24 (9)	0.005
In2	0.56923 (15)	0.25	0.61152 (11)	0.31 (9)	0.995
Er2	0.56923 (15)	0.25	0.61152 (11)	0.31 (9)	0.005
O1	0.2911 (12)	0.25	0.3322 (12)	0.65 (18)	1
O2	0.1209 (12)	0.75	0.5207 (10)	0.65 (18)	1
O3	0.0215 (14)	0.75	0.2777 (11)	0.65 (18)	1
O4	0.4207 (13)	0.75	0.5793 (10)	0.65 (18)	1

Table III. Main Bond Lengths (Å) of Compounds (1) and (2)

$SrIn_2O_4$: $0.1Yb^{3+}/0.01Er^{3+}$ (**1**)			
Sr—O1^{i}	2.689 (7)	In1—O2^{ii}	2.197 (8)
Sr—O2	2.539 (6)	In1—O3	2.148 (5)
Sr—O3^{ii}	2.687 (10)	In2—O1^{iv}	2.248 (6)
Sr—O3^{iii}	2.797 (9)	In2—O3^{iii}	2.183 (8)
Sr—O4	2.508 (7)	In2—O4	2.247 (6)
In1—O1	2.131 (8)	In2—O4^{v}	2.213 (8)
In1—O2	2.245 (6)		
$SrIn_2O_4$: $0.01Er^{3+}$ (**2**)			
Sr—O1^{i}	2.650 (11)	In1—O2^{ii}	2.214 (12)
Sr—O2	2.547 (9)	In1—O3	2.191 (9)
Sr—O3^{ii}	2.739 (14)	In2—O1^{iv}	2.230 (8)
Sr—O3^{iii}	2.702 (14)	In2—O3^{iii}	2.108 (13)
Sr—O4	2.523 (10)	In2—O4	2.222 (9)
In1—O1	2.185 (12)	In2—O4^{v}	2.196 (11)
In1—O2	2.223 (8)		

Symmetry codes: (i) $-x + 1/2, -y, z + 1/2$; (ii) $-x, -y + 1, -z + 1$; (iii) $-x + 1/2, -y + 1, z + 1/2$; (iv) $-x + 1, -y, -z + 1$; (v) $-x + 1, -y + 1, -z + 1$.

Figure 4(a) displays the UC luminescence spectra of as-prepared $SrIn_2O_4$: $0.1Yb^{3+}/xEr^{3+}$ and $SrIn_2O_4$: $0.01Er^{3+}$ phosphors upon 980 nm laser excitation, and the insets shows the variation in UC emission intensities (Er^{3+}, at 663 and 550 nm) of these corresponding samples. As can be seen that, the sample $SrIn_2O_4$: $0.01Er^{3+}$ where no Yb^{3+} was doped showed very weak UC luminescence. For $SrIn_2O_4$: $0.1Yb^{3+}/xEr^{3+}$, strong green and red UC emissions with the peak centered at 525, 550, and 663 nm were observed, which are assigned to the characteristic Er^{3+} ion transitions of $^2H_{11/2}\rightarrow{}^4I_{15/2}$, $^4S_{3/2}\rightarrow{}^4I_{15/2}$, and $^4F_{9/2}\rightarrow{}^4I_{15/2}$, respectively.[1-4,20-22] Compared with $SrIn_2O_4$: $0.01Er^{3+}$, luminescent intensity of $SrIn_2O_4$: $0.1Yb^{3+}/0.01Er^{3+}$ increased greatly, indicating the addition of Yb^{3+} ions improved the UC properties for these materials. UC emission intensities of red emission (663 nm) and green emission (550 nm) arrived maximum in $SrIn_2O_4$: $0.1Yb^{3+}/0.03Er^{3+}$ and $SrIn_2O_4$: $0.1Yb^{3+}/0.01Er^{3+}$, respectively. The luminescent intensities of $SrIn_2O_4$: $0.1Yb^{3+}/xEr^{3+}$ increase first and then decrease at either 663 or 550 nm with the increasing Er^{3+} concentration, suggesting that the concentration quenching occurred. The over-doped Er^{3+} ions lead to the decreasing distance between Er^{3+} and Yb^{3+}(or Er^{3+}) ions, which limited the energy transfer (ET) of $Yb^{3+}\rightarrow Er^{3+}$, followed by decreasing luminescent intensity of Er^{3+} ions.[10] In addition, Fig. 4(b) gives the diffuse reflection spectra of pure $SrIn_2O_4$, $SrIn_2O_4$: $0.03Er^{3+}$, $SrIn_2O_4$: $0.1Yb^{3+}$, and $SrIn_2O_4$: $0.1Yb^{3+}/0.03Er^{3+}$ samples. Single Er^{3+}-doped $SrIn_2O_4$ shows apparent absorption band at 522, 653, 796 nm, however, the absorption at 978 nm was slight. Therefore, the weak UC luminescence may be owing to the ground absorption of Er^{3+} and phonon energy. In contrast, the Yb^{3+} single-doped $SrIn_2O_4$ only possessed strong absorption at 899 and 978 nm, which were assigned to the characteristic $^2F_{7/2}\rightarrow{}^2F_{5/2}$ transition of Yb^{3+} ions. For $SrIn_2O_4$: $0.1Yb^{3+}/0.03Er^{3+}$, absorption band at 522, 653, 796 nm and strong absorption at 899 and 978 nm were observed simultaneously. Considering that Yb^{3+}/Er^{3+} codoped $SrIn_2O_4$ showed much higher UC intensity than single Er^{3+}-doped $SrIn_2O_4$, it is reasonable to believe that the increasing absorption in 980 nm is mainly from the energy state transition of Yb^{3+} ions, and ET of $Yb^{3+}\rightarrow Er^{3+}$ played a significant role in the UC luminescent process.

As we known, the phonon energy of host has important influence on the UC luminescent efficiency. Therefore, FTIR spectra of pure $SrIn_2O_4$ and $CaIn_2O_4$ were studied and shown in Fig. 5(a). Compared with $CaIn_2O_4$ (489, 637 cm^{-1}), the strong absorption bands of $SrIn_2O_4$ (467, 598 cm^{-1}) were shifted to the smaller wave number, suggesting that the phonon energy of $SrIn_2O_4$ (467 cm^{-1}) was lower than that of $CaIn_2O_4$.[10] Moreover, because of the difference of Sr^{2+} and Ca^{2+}, Yb^{3+}/Er^{3+} codoped $SrIn_2O_4$ maybe show more excellent luminescent properties than Yb^{3+}/Er^{3+} codoped $CaIn_2O_4$, and this was proved by the comparison of UC luminescence spectra of $0.1Yb^{3+}/xEr^{3+}$ (x = 0.005, 0.01, 0.03) codoped $SrIn_2O_4$ and $CaIn_2O_4$ samples in Fig. 5(b). From the inset of Fig. 5(b), the luminescent intensity of either $SrIn_2O_4$ or $CaIn_2O_4$ raised with the increasing of Er^{3+} (from 0.005 to 0.03), however, the intensities of Yb^{3+}/Er^{3+} codoped $SrIn_2O_4$ were higher than that of $CaIn_2O_4$ for the corresponding concentration.

The UC emission intensity (I_{em}) depends on the pumping laser power (P_{pump}) which follows the relation:

$$I_{em} \propto (P_{pump})^n \tag{1}$$

where n is the number of pump photons required for the transition from ground state to the upper emitting state. The value n can be obtained from the slope of a straight line that resulted from log I_{em} versus log P_{pump}.[5,20,25] Figure 6 shows the UC emission spectra of $SrIn_2O_4$: $0.1Yb^{3+}/0.01Er^{3+}$ with different pumping powers and the inset shows the dependence of green and red UC emission intensities upon pumping power. The calculated slopes were 2.09 ± 0.07 for the red emission(663 nm: $^4F_{9/2} \rightarrow {}^4I_{15/2}$) and 1.81 ± 0.06 for

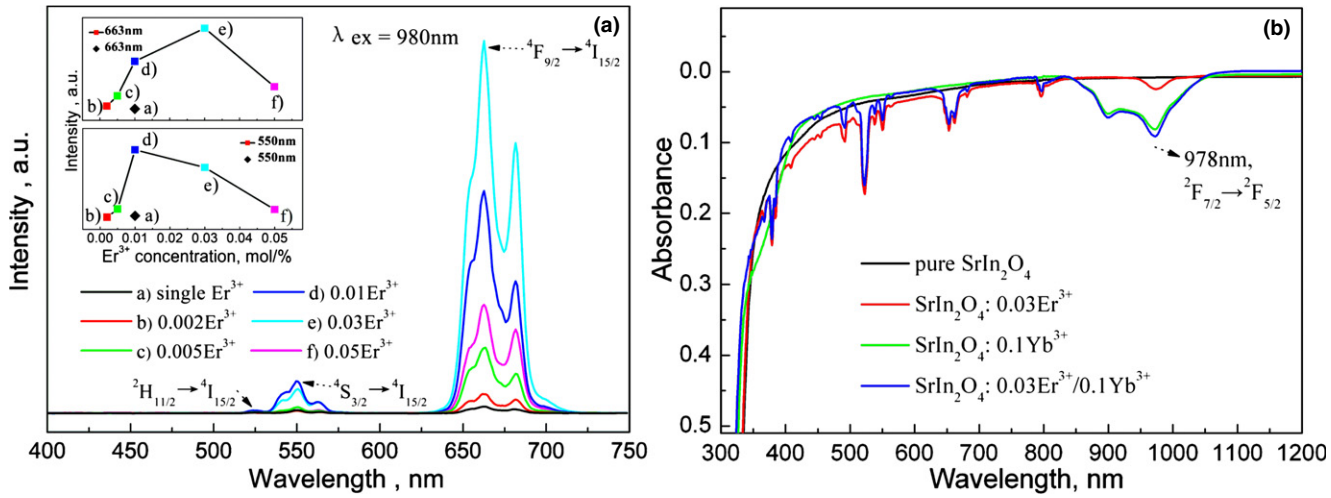

Fig. 4. (a) UC luminescence spectra of $SrIn_2O_4$: $0.1Yb^{3+}/xEr^{3+}$ (x = 0.002, 0.005, 0.01, 0.03, 0.05) and $SrIn_2O_4$: $0.01Er^{3+}$ samples under 980 nm laser excitation, and the inset shows the variation in UC emission intensities (Er^{3+}, at 665 nm and 550 nm) of these corresponding samples; (b) The diffuse reflection spectra of pure $SrIn_2O_4$, $SrIn_2O_4$: $0.03Er^{3+}$, $SrIn_2O_4$: $0.1Yb^{3+}$, and $SrIn_2O_4$: $0.1Yb^{3+}/0.03Er^{3+}$ samples.

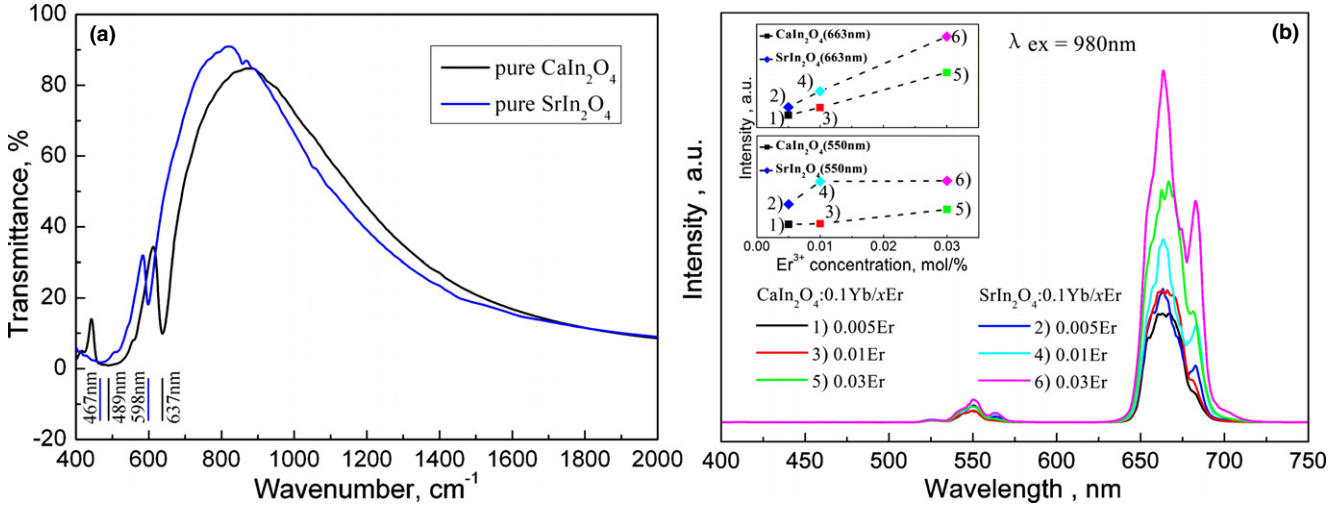

Fig. 5. (a) FTIR spectra of pure $SrIn_2O_4$ and $CaIn_2O_4$; (b) Comparison of UC luminescence spectra of $0.1Yb^{3+}/xEr^{3+}$ (x = 0.005, 0.01, 0.03) codoped $SrIn_2O_4$ and $CaIn_2O_4$ samples under 980 nm laser excitation.

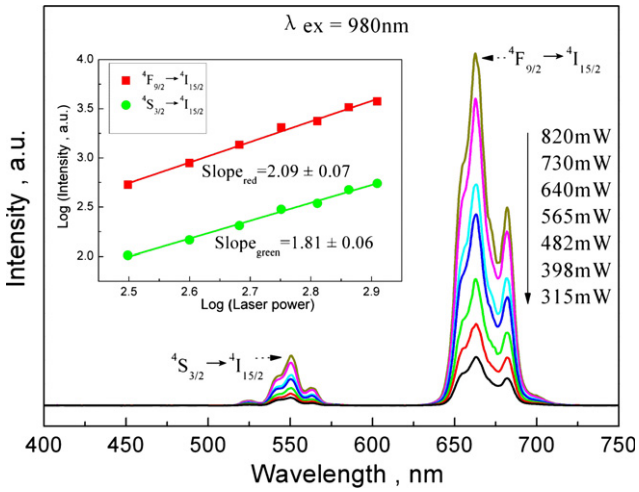

Fig. 6. UC emission spectra of $SrIn_2O_4$: $0.1Yb^{3+}/0.01Er^{3+}$ with different pumping powers and the inset shows the dependence of green and red UC emission intensities upon pumping powers.

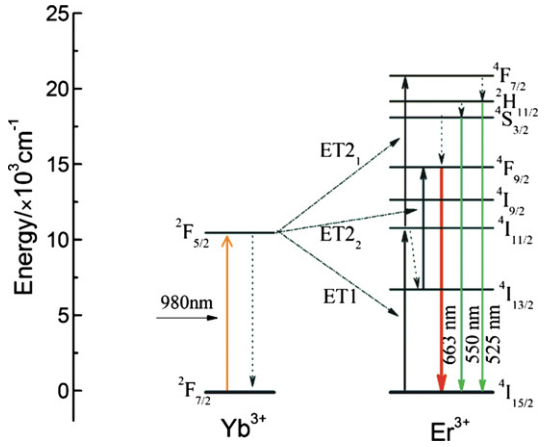

Fig. 7. Energy level diagram and the proposed UC luminescence mechanism in $SrIn_2O_4$: Yb^{3+}/Er^{3+} phosphors.

the green emission(550 nm: $^4S_{3/2} \rightarrow {}^4I_{15/2}$), indicating that the UC luminescence in Yb^{3+}/Er^{3+} codoped $SrIn_2O_4$ mainly is the two-photon process.

According to the above-mentioned photon process, the energy level diagram of Er^{3+} and Yb^{3+} ions and the proposed UC luminescent mechanism to produce green and red emission have been reveals in Fig. 7. First of all, infrared photon near 980 nm wavelength are absorbed by Yb^{3+} ions and elevates Yb^{3+} ion from $^2F_{7/2}$ to $^2F_{5/2}$ energy level. Then, the energy is transferred to the Er^{3+} ions, because nonradiative energy transition (ET) from $^2F_{5/2}$ of Yb^{3+} to $^4I_{11/2}$ of Er^{3+} is resonant or near resonant and thus very efficient. The first ET promotes an Er^{3+} ion from the $^4I_{15/2}$ to $^4I_{11/2}$ level, and the second ET elevates the Er^{3+} ion from the $^4I_{11/2}$ to the $^4F_{7/2}$ if the $^4I_{11/2}$ is already populated. Er^{3+} ions in the $^4F_{7/2}$ state decay nonradiatively to slight lower energy states of $^2H_{11/2}$, $^4S_{3/2}$, so that the green light of 525 and 550 nm are emitted by Er^{3+} transition from $^2H_{11/2}$ to $^4I_{15/2}$ and $^4S_{3/2}$ to $^4I_{15/2}$ state, respectively. At the same time, Er^{3+} can decay to the $^4F_{9/2}$ via a nonradiative relaxation process, and then the red light (663 nm) was observed through the radiative transition from $^4F_{9/2}$ to $^4I_{15/2}$.[17,20,22,25] Moreover, Er^{3+} in $^4I_{11/2}$ level can relax nonradiatively to the lower excited state of $^4I_{13/2}$, thus the second ET also can be taken place from the $^4I_{13/2}$ and promote Er^{3+} to $^4I_{9/2}$ level. The relative UC intensity of red light is larger than green light, indicating that the population of the $^4F_{9/2}$ was larger than $^2H_{11/2}$ and $^4S_{3/2}$ levels, and this is probably influenced by some factors such as phase structure and lattice defects.[24]

IV. Conclusions

Yb^{3+} and/or Er^{3+} codoped $SrIn_2O_4$ were synthesized by a traditional solid-state reaction method. $SrIn_2O_4$ was proved to be an excellent up-conversion (UC) host to exhibits UC luminescence which is better than $CaIn_2O_4$ owing to its lower phonon energy. Yb^{3+}/Er^{3+} codoped $SrIn_2O_4$ compounds showed great improvement in UC luminescence, with strong emission in the green (525, 550 nm) and red (663 nm) spectral ranges, which were assigned to the energy level transitions of $^2H_{11/2}\rightarrow{}^4I_{15/2}$, $^4S_{3/2}\rightarrow{}^4I_{15/2}$ and $^4F_{9/2}\rightarrow{}^4I_{15/2}$ of Er^{3+}, respectively. The structures of $SrIn_2O_4$: $0.01Er^{3+}$ and $SrIn_2O_4$: $0.1Yb^{3+}/0.01Er^{3+}$ were refined by the Rietveld method and the larger unit cell parameters and unit cell volume of the doped compounds reveals that In^{3+} sites were substituted successfully by Yb^{3+} and/or Er^{3+} ions. From the FTIR spectra, $SrIn_2O_4$ possessed smaller phonon energy than $CaIn_2O_4$, indicating that Yb^{3+} and/or Er^{3+} codoped $SrIn_2O_4$ phosphors can achieve more high-efficiency UC emission than their $CaIn_2O_4$ counterparts. This indication was testified by the comparison of UC luminescence spectra of Yb^{3+}/

Er^{3+} codoped $SrIn_2O_4$ and $CaIn_2O_4$. The pumping powers study indicates that the energy transfer of $Yb^{3+} \rightarrow Er^{3+}$ in the $SrIn_2O_4$ host is a two-photon process.

Acknowledgment

This present work was supported by the National Natural Science Foundations of China (grant no. 51202226), the Fundamental Research Funds for the Central Universities (grant nos. 292014125,2652013128, 2652013043), and the Research Fund for the Doctoral Program of Higher Education of China (grant no. 20130022110006).

References

[1]F. Auzel, "Upconversion and Anti–Stokes Processes with f and d Ions in Solids," *Chem. Rev.*, **104**, 139–73 (2004).

[2]F. Wang, R. R. Deng, J. Wang, Q. X. Wang, Y. Han, H. M. Zhu, X. Y. Chen, and X. G. Liu, "Tuning Upconversion Through Energy Migration in Core–Shell Nanoparticles," *Nat. Mater.*, **10**, 968–73 (2011).

[3]Y. H. Wang and J. Ohwaki, "New Transparent Vitroceramics Codoped with Er^{3+} and Yb^{3+} for Efficient Frequency Upconversion," *Appl. Phys. Lett.*, **63**, 3268–70 (1993).

[4]F. Wang and X. G. Liu, "Recent Advances in the Chemistry of Lanthanide–Doped Upconversion Nanocrystals," *Chem. Soc. Rev.*, **38**, 976–89 (2009).

[5]J. Zhang, Y. H. Wang, L. N. Guo, and P. Y. Dong, "Up–Conversion Luminescence and Near–Infrared Quantum Cutting in $Y_6O_5F_8$: RE^{3+} (RE = Yb, Er, and Ho) with Controllable Morphologies by Hydrothermal Synthesis," *Dalton T*, **42**, 3542–51 (2013).

[6]Q. Zhang, B. Zhu, Y. X. Zhuang, G. R. Chen, X. F. Liu, G. Zhang, J. R. Qiu, and D. P. Chen, "Quantum Cutting in Tm^{3+}/Yb^{3+}–Codoped Lanthanum Aluminum Germanate Glasses," *J. Am. Ceram. Soc.*, **93**, 654–7 (2010).

[7]F. M. Li, L. Li, C. F. Guo, T. Li, H. M. Noh, and J. H. Jeong, "Up-Conversion Luminescence Properties of Yb^{3+}-Ho^{3+} Co-Doped $CaLa_2ZnO_5$.," *Ceram. Int.*, **40**, 7363–6 (2014).

[8]J. W. Tang, Z. G. Zou, and J. H. Ye, "Effects of Substituting Sr^{2+} and Ba^{2+} for Ca^{2+} on the Structural Properties and Photocatalytic Behaviors of $CaIn_2O_4$.," *Chem. Mater.*, **16**, 1644–9 (2004).

[9]J. H. Ye, Z. G. Zou, M. Oshikiri, A. Matsushita, M. Shimoda, M. Imai, and T. Shishido, "A Novel Hydrogen–Evolving Photocatalyst $InVO_4$ Active Under Visible Light Irradiation," *Chem. Phys. Lett.*, **356**, 221–6 (2002).

[10]T. Li, C. F. Guo, and L. Li, "Up–Conversion Luminescence of Er^{3+}–Yb^{3+} Co–Doped $CaIn_2O_4$," *Opt. Express*, **21**, 18281–9 (2013).

[11]T. Li, C. F. Guo, Y. M. Yang, L. Li, and N. Zhang, "Efficient Green Up–Conversion Emission in Yb^{3+}/Ho^{3+} Co–Doped $CaIn_2O_4$," *Acta Mater.*, **61**, 7481–7 (2013).

[12]A. Baszczuk, M. Jasiorski, M. Nyk, J. Hanuza, M. Maczka, and W. Strek, "Luminescence Properties of Europium Activated $SrIn_2O_4$," *J. Alloy. Compd.*, **394**, 88–92 (2005).

[13]R. V. Schenk and H. Mueller Buschbaum, "Kristallstrukturuntersuchung an $SrIn_2O_4$," *Z. Anorg. Allg. Chem.*, **398**, 24–30 (1973).

[14]R. D. Shannon, "Revised Effective Ionic Radii and Systematic Studies of Interatomic Distances in Halides and Chalcogenides," *Acta Cryst. A*, **32**, 751–67 (1976).

[15]H. L. Wang and L. H. Tian, "Luminescence Properties of $SrIn_2O_4$:Eu^{3+} Incorporated with Gd^{3+} or Sm^{3+} Ions," *J. Alloy. Compd.*, **509**, 2659–62 (2011).

[16]F. S. Kao, "A Study on the Luminescent Properties of New Green–Emitting $SrIn_2O_4$: XTb Phosphor," *Mater. Chem. Phys.*, **76**, 295–8 (2002).

[17]D. Matsuura, "Red, Green, and Blue Upconversion Luminescence of Trivalent–Rare–Earth Ion–Doped Y_2O_3 Nanocrystals," *Appl. Phys. Lett.*, **81**, 4526–8 (2002).

[18]R. T. Wegh, E. V. D. van Loef, and A. Meijerink, "Visible Quantum Cutting Via Downconversion in $LiGdF_4$: Er^{3+}, Tb^{3+} Upon Er^{3+} ^4f $^{11} \rightarrow ^4f$ ^{10} 5d Excitation," *J. Lumin.*, **90**, 111–22 (2000).

[19]X. Zou and T. Izumitani, "Spectroscopic Properties and Mechanisms of Excited State Absorption and Energy Transfer Upconversion for Er^{3+}–Doped Glasses," *J. Non–Cryst. Solids*, **162**, 68–80 (1993).

[20]Z. G. Xia, P. Du, and L. B. Liao, "Facile Hydrothermal Synthesis and Upconversion Luminescence of Tetragonal Sr_2LnF_7: Yb^{3+}/Er^{3+} (Ln=Y, Gd) Nanocrystals," *Phys. Status Solidi A*, **210**, 1734–7 (2013).

[21]C. N. Zhong, P. P. Yang, X. B. Li, C. X. Li, D. Wang, S. L. Gai, and J. Lin, "Monodisperse Bifunctional Fe_3O_4@$NaGdF_4$:Yb/Er@$NaGdF_4$:Yb/Er Core–Shell Nanoparticles," *RSC Adv.*, **2**, 3194–7 (2012).

[22]J. H. Zeng, J. Su, Z. H. Li, R. X. Yan, and Y. D. Li, "Synthesis and Upconversion Luminescence OF Hexagonal–Phase $NaYF_4$: Yb, Er^{3+} Phosphors of Controlled Size and Morphology," *Adv. Mater.*, **17**, 2119–23 (2005).

[23]F. Wang and X. G. Liu, "Emission from Lanthanide–Doped $NaYF_4$ Nanoparticles," *J. Am. Chem. Soc.*, **130**, 5642–3 (2008).

[24]Z. L. Wang, J. H. Hao, and H. L. W. Chan, "Down- and Up-Conversion Photoluminescence, Cathodoluminescence and Paramagnetic Properties of $NaGdF_4$: Yb^{3+}, Er^{3+} Submicron Disks Assembled from Primary Nanocrystals," *J. Mater. Chem.*, **20**, 3178–85 (2010).

[25]Z. G. Xia, J. Li, Y. Luo, and L. B. Liao, "Comparative Investigation of Green and Red Upconversion Luminescence in Er^{3+} Doped and Yb^{3+}/Er^{3+} Codoped LaOCl," *J. Am. Ceram. Soc.*, **95**, 3229–34 (2012).

[26]Bruker AXS TOPAS V4, General Profile and Structure Analysis Software for Powder Diffraction Data – User's Manual. Bruker AXS, Karlsruhe, Germany, 2008. □